GENERAL EXPERIMENTAL TECHNIQUE

EXPERIMENTAL SETUP FOR PROBING PLASMA OF HIGH-VOLTAGE SPARK GAP WITH LASER CONTROL

©2025 A. I. Lipchak,*, N. B. Volkov, I. A. Zhuravlev

Institute of Electrophysics

Ural branch of the Russian Academy of Sciences

Russia, Ekaterinburg

**e-mail:lipchak@iep.uran.ru*

Received July 22, 2024

Revised October 18, 2024

Accepted November 19, 2024

Abstract. The article presents a technique and a setup implementing it for optical probing of pulsed plasma initiated by YAG:Nd3+ laser radiation in a high-voltage gas switch with laser control, which can be used as a primary switch of a high-current high-voltage pulsed electron accelerator-generator of the RADAN type. The studies were conducted in a natural atmosphere. The first results of measuring the dynamics of the laser radiation absorption coefficient in plasma obtained on this setup are presented. These data indicate the implementation of conditions for nonlinear absorption of laser radiation by plasma at excitation energy densities greater than 240 J/cm2; they will allow developing recommendations for choosing the parameters of spark gap triggering in order to minimize the instability of its switching on.

DOI: 10.31857/S00328162250118e8

1. INTRODUCTION

Laser plasma is a key element determining the stability and accuracy of switching on high-pressure gas-discharge switches with optical control [1, 2]. Despite the decades since the appearance of such devices, interest in their improvement is determined by both their unique properties and the complexity of the processes occurring in them. Their advantages include complete isolation of the control circuits from the controlled ones and the possibility of preliminary creation of a long plasma channel with high conductivity, having various configurations [3, 4]. This stimulates activity in the study of laser plasma under various conditions at the present time [5, 6].

2. EQUIPMENT AND MEASUREMENT METHODOLOGY

The main element of the installation was a previously developed optically-controlled spark gap for a high-voltage pulse generator-accelerator of the RADAN type. It contains two polished stainless steel electrodes, designed as bodies of revolution with a Rogowski profile, which can be positioned at a distance of 3-10 mm from each other (Fig. 1). A 2 mm diameter hole was drilled along the axis in the cathode for introducing laser radiation. The radiation was focused on the anode by a lens with a focal length of 100 mm. It has been experimentally established [7] that this configuration ensures minimal instability (jitter) of switching when the voltage level on the gas gap is 90-95% of the self-breakdown voltage and with voltage rise time of about 10^{-6} s ($dU/dt \sim 10^{11}$ V/s), typical for charging a double forming line of a high-current high-voltage pulse generator-accelerator of the RADAN type [8]. Fig. 2 shows the schematic diagram of the experimental setup. The first harmonic radiation of YAG:Nd^{3+}-laser with λ λ = 1064 nm was used to form the plasma. Along with this, the second harmonic of this laser, λ λ =532 nm, was used for plasma probing in the direction normal to the axis of the igniting pulse. The diaphragmed beam passed through the region of minimum distance between the electrodes . The aperture of the probing pulse was limited by a diaphragm with a diameter D =0.8 mm (see Fig. 2, bottom inset). This paper presents the results of plasma probing at a distance $r = D/2$ from the anode to the axis of the probing pulse aperture – so that it "slid" along the anode.

Fig. 1. Optically-controlled spark gap for a high-voltage pulse generator-accelerator of the RADAN type **:** *1* – probing laser pulse, *2* – ...

Fig. 2. Experimental setup, top view

The reason for using the second harmonic is based on the following known relation [9], which determines the threshold electron concentration above which probing is impossible because radiation cannot pass through the plasma:

$$n_{cr} = \frac{\omega^2 m_e \varepsilon_0}{e^2}, \qquad (1)$$

where ε_0 is the permittivity, m_e is the electron mass, e is the elementary charge, $\omega = 2\pi c/\lambda$, c is the speed of light in vacuum, λ is the wavelength of laser radiation. It can be seen that the second harmonic allows probing plasma in a wider range of electron concentrations. Another problem that needed to be solved was accounting for laser pulse instabilities from pulse to pulse. This effect is mainly caused by beating of longitudinal modes in the multimode regime of laser radiation generation [10, 11], which is especially noticeable at low pump levels of the laser active medium. Therefore, it is necessary to register reference copies of the pulse unaltered by plasma to compare them with pulses

that have passed through it. For this purpose, the optical scheme provided for splitting the second harmonic pulse with a beam splitter into reference and probe pulses. Subsequently, these pulses can be registered by a single common photodetector. A single UPD-50-UP photodiode with a rise/fall time of 50 ps was used in this work. In this case, a delay of about 100 ns is required to separate two laser pulses with a duration of about 45 ns in time. To obtain this delay, an air delay line with a length of about 30 m can be used, but this would significantly increase the dimensions of the experimental stand. Another possible option is to use 12-14 retroreflectors (we proceed from the typical length of an optical bench of 2.5-3.0 m), but the use of each would inevitably lead to distortion of the laser beam geometry and an increase in its divergence. An optical fiber with a length of about 20 m can also be used to delay the laser beam. At the same time, the overall size of the stand can be reduced by coiling this optical fiber into a ring. However, optical fibers for transmitting multimode laser pulses have known limitations. It is known that mode dispersion is the dominant factor in distorting the shape of laser pulses in light guides [12], since the optical path length for different modes varies, and higher modes travel a longer optical path than lower ones.

To overcome these limitations, a combined approach was applied. A shortened air delay line with eight retroreflectors with a total length of 15 m and a 12 m quartz fiber were used. The probe and reference pulses were combined and recorded by a single photodiode (upper *BS* , Fig. 2) to eliminate accounting for differences in the hardware functions of different sensors. The energy of the igniting pulse of the first harmonic E_i varied in the range of 50-100 mJ.

The result of testing the probing system without plasma formation is shown in Fig. 3. It demonstrates the operation of the combined delay line. Fig. 4 shows the ratio of the reference pulse I_{ref} to the probe pulse I_{prob} in the absence of probed plasma in the discharger. Except for the initial and final phases with a low signal-to-noise ratio, the measurements give an absorption coefficient close to one (Fig. 4, curve *3*). Thus, the distortion of the probe signal passing through the delay line appears insignificant compared to the distortion of the probe signal introduced by the plasma formed by a pulse even with the minimum energy E_i =55 mJ (Fig. 5).

Fig. 3. Result of testing the probing system without plasma formation: *1* – non-delayed probe pulse, *2* – delayed reference pulse without plasma.

Fig. 4. Ratio of reference pulse I_{ref} to probe pulse I_{prob} in the absence of probed plasma in the discharger: *1* – non-delayed probe pulse, *2* – ...

Fig. 5. Distortion of the probe signal introduced by plasma formed by a pulse with minimum energy E_i=55 mJ : *1* – probe pulse transmitted through plasma,

3. RESULTS AND DISCUSSION

Obviously, we can introduce a plasma absorption coefficient as the ratio of the reference signal intensity to the probe signal: $K(t)=I_{ref}/I_{prob}$ (Fig. 5, curve *3*). It was measured for a fixed set of pulse energies E_i = 55.0, 65.5, 76.0, 85.5, 95.5 mJ. The data were processed over a series of N=20 pulses. Its mean value $K_m(t)$:

$$K_m = \left(\sum_{j=1}^{N} \left(K_j \right) \right) \cdot N^{-1}, \quad N = 20 \tag{2}$$

and confidence interval ΔK for probability p =0.95 and Δt =0.4 ns [13], which was considered as the jitter of the process (by analogy with what is written in [14]).

Fig. 6 shows the superposition of 20 signals obtained during a series of measurements for a fixed energy of the triggering laser pulse (E_i=55 mJ). It can be seen that the scatter of the absorption coefficient begins to increase significantly after 35 ns from the beginning of the laser pulse. Examples of calculating $K_m(t)$ and ΔK for different laser pulse energies are presented in Fig. 7, 8, curves *1* and *2* respectively.

Fig. 6. Superposition of 20 signals obtained during a series of measurements at a fixed energy of the triggering laser pulse E_i=55 mJ, $K(t)= I_{ref}/ I_{prob}$.

Fig. 7. Calculation of $K_m(t)$ and ΔK at laser pulse energy E_i=55 mJ: *1* – average absorption coefficient K_m (left axis), *2* – ΔK (right axis).

Fig. 8. Calculation $K_m(t)$ and ΔK at laser pulse energy E_i=95.5 mJ.: *1* – average absorption coefficient K_m (left axis), **2** – ΔK (right axis).

The dependence of the absorption coefficient at the initial phase of the laser pulse with varying pulse energy is shown in Fig. 9. It can be seen that in the first approximately 15 ns, the absorption coefficient is practically independent of the pulse energy E_i . Subsequently, the nature of the dependence for different pulse energies differs significantly. At pulse energy $E_i \geq$ 76 mJ (which corresponds to an energy density of about 240 J/cm ^{2} or peak power density $p_{max} \approx 5.7 \cdot 10^{10}$ W/cm ^{2} with a focusing spot diameter $d \sim$ 0.01 cm) this dependence becomes non-monotonic.

Fig. 9. Dependence of the absorption coefficient K_m on time and laser pulse energy.

First, this is related to *plasma clearing* [15]. It is noted that when laser radiation is absorbed, the temperature of the plasma's electron component increases first. This increase promotes the ionization of excited atoms during collisions with electrons within a time of about 10^{-11} s or less. The temperature increase also enhances the excitation of atoms from the ground state during electron impacts. In the case of a nanosecond laser pulse, the excitation of atoms from the ground state does not have time to occur, and the population of atomic levels decreases as a result. At the same time, a new quasi-equilibrium state is established, in which there is an equilibrium between the electron component of the plasma and excited atoms. However, there is no equilibrium between excited and unexcited atoms. Thus, the concentration of excited atoms, which are the main absorbers of laser radiation, becomes lower, leading to an effective reduction in radiation absorption by the plasma.

Secondly, when exceeding the power density level $p \geq 5 \cdot 10^{10}$ W/cm^2, conditions arise for the manifestation of nonlinear absorption of laser radiation, associated with the deviation of their distribution from Maxwellian, which, in turn, leads to a decrease in the probability of radiation absorption due to the inverse bremsstrahlung effect [16]. As a criterion here, the equality of the average kinetic energy of an electron and its thermal energy is conditionally chosen. The velocity that an electron acquires in the field of a light wave on average over one period is proportional to $1/\omega$. In turn, this means that the specified criterion for lower-frequency radiation of the first harmonic of laser radiation is realized earlier, at lower power densities. Nevertheless, we note that the experimentally obtained value of the peak power density, starting from which non-monotonic behavior of the absorption coefficient is observed, agrees well with the values obtained in [16].

These mechanisms can lead to a decrease in the absorption coefficient, which is manifested in experiments when the pulse energy increases (Fig. 9, curves *3* - *5*). We also note that, unlike in [15], the presented experimental technique allows studying this phenomenon in dynamics during a pulse without time integration.

The effect described above apparently can play a significant role in forming the non-monotonic dependence of instability in a laser-triggered spark gap, observed particularly in work [7]. Unlike experiments on plasma formation in pure gas without a target [16], the nonlinear behavior of radiation absorption coefficient during its formation on a solid surface acts as feedback. In general terms, *N* - shaped characteristic of such feedback is, generally speaking, a necessary condition for oscillation formation [17]. As shown in Fig. 9 (curves *3-5* , such feedback form manifests itself as laser radiation intensity increases. This statement is supported by statistical instability of absorption in the final phase of the pulse, which can be considered as absorption coefficient jitter (Fig. 10). For laser pulse energies where nonlinear absorption conditions are not realized (curves *1* , *2* , the jitter is noticeably smaller

than in cases where they occur (curves *3* - *5*). This provides additional evidence of this effect's significant contribution to the operational instability of laser-triggered gas spark gaps. Note that this may not be the only phenomenon determining the instability of transition to high conductivity state in such devices [18, 19].

Fig. 10. Dependence of jitter of absorption coefficient on time and laser pulse energy.

4. CONCLUSION

Using the created experimental setup, a study was conducted on plasma absorption of nanosecond laser pulse second harmonic with λ =5 32 nm. The dynamics of plasma absorbing capacity was studied with variations in the ignition pulse energy. Measurements of the absorbing capacity confirmed the appearance of nonlinear absorption at energy densities above 240 J/cm ^{2} , which leads to instability of the plasma's absorbing capacity and, consequently, deteriorates the temporal characteristics of triggering of the high-voltage discharge switch with laser control. The developed experimental setup will be further used to verify this interpretation, and the obtained data will be used to optimize the parameters of the triggering laser pulse. In particular, experimental studies of these effects are planned at elevated pressures and with variation of the quasi-static electric field strength in the range typical for discharge switches of high-current high-voltage pulse generator-accelerators of the RADAN type, in order to find conditions for implementing minimal jitter in the activation of such devices.

REFERENCES

1. *Pendleton W.K., Guenther A.H.* // Rev. Sci. Instrum. 1965. V. 36. P. 1546. https://doi.org/10.1063/1.1719388
2. *Alcock A.J., Richardson M.C., Leopold K.* // Rev. Sci. Instrum. 1970. V. 41. P. 1028. https://doi.org/10.1063/1.1684689
3. *Rosenthal E., Larkin I., Goffin A., Produit T., Schroeder M., Wolf J., Milchberg H.* // Opt. Express. 2020. V. 28. P. 24599. https://doi.org/10.1364/OE.398836
4. *Dehne K., Higginson A., Wang Y., Tomasel F., Capeluto M., Shlyaptsev V., Rocca J.* // Opt. Express. 2024. V. 32. P.16164. https://doi.org/10.1364/OE.506547
5. *Zhou W.D., Guo Y.H., Zhang R.R.* // Front Phys. 2020. V. 15. P. 52201. https://doi.org/10.1007/s11467-020-0969-1

6. *Shangguan S., Zhang J., Li Z., Shi W., Wang W., Qi D., Zheng H.* // Sci. China Technol. Sci. 2024. V. 67. P.73. https://doi.org/10.1007/s11431-023-2499-0
7. *Lipchak A.I., Barakhvostov S.I.* // PTE. 2021. No. 3. P. 40. https://doi.org/10.31857/S0032816221030216
8. *Mesyats G.A., Yalandin M.I.* // UFN. 2005. V. 175. No. 3. P. 225
9. *Michel P.* Fundamentals of Optics and Plasma Physics, Introduction to Laser-Plasma Interactions. Graduate Texts in Physics. Cham: Springer, 2023. https://doi.org/10.1007/978-3-031-23424-8_1
10. *Paschotta R.* Field Guide to Laser Pulse Generation. Bellingham, WA.: SPIE Press, 2008. https://doi.org/10.1117/3.800629
11. *Rand D., Hybl J., Fan T.Y.* Cryogenic lasers, Handbook of Solid-State Lasers. Cambridge: Woodhead Publ., 2013. https://doi.org/10.1533/9780857097507.2.525
12. *Koike Y., Koike K.* // Polymer Science: A Comprehensive Reference. 2012. V. 8. P. 283. https://doi.org/10.1016/B978-0-444-53349-4.00209-0
13. State system for ensuring the uniformity of measurements. Direct multiple measurements. Methods of measurement results processing. Main principles. Moscow: Standardinform, 2013. GOST R 8.736-2011.
14. *Lipchak A.I., Volkov N.B., Turmyshev I.S., Chingina E.A*. // Bulletin of the Russian Academy of Sciences Physics. 2024. V. 87. (Suppl 2). S222. https://doi.org/10.1134/S1062873823704646
15. *Generalov N.A., Kozlov G.I., Raizer Yu.P.* // PMTF. 1970. № 3. P. 27.
16. *Prokhorov A.M., Konov V.I., Ursu I., Mikhailescu I.N*. Interaction of laser radiation with metals. Moscow: Nauka, 1988. P. 242.
17. *Wey T.A., Ogborn L.L.* // ECE Technical Reports. 1995. № 12. P. 169. http://docs.lib.purdue.edu/ecetr/169
18. *Volkov N.B., Lipchak A.I.* // Condensed Matter. 2022. V. 7(4). P. 61. https://doi.org/10.3390/condmat7040061
19. *Volkov N.B., Lipchak A.I.* // Condensed Matter. 2023 V. 8(3). P. 70. https://doi.org/10.3390/condmat8030070

FIGURE CAPTIONS

Fig. 1. Optically controlled spark gap for high-voltage pulse generator-accelerator of RADAN type **:** *1* – probing laser pulse, *2* – ignition laser pulse, *3* – anode, *4* – cathode, *5* – laser plasma.

Fig. 2. Experimental setup, top view: *1* – splitting unit λ =532, nm, *2* – unit for inputting and focusing radiation λ =1064 nm into the discharger; *3* , *4* – sets of retroreflectors, *5* – unit for inputting the reference pulse into the optical fiber, *6* – pulse combining unit, *7* – probe pulse, *8* – reference pulse,

9 – delay line, *BS* – beam splitters, *RP* – reflecting prism, *L* – lenses, cathode not shown. In the upper inset – plasma formation unit, cathode not shown. Lower inset – probing geometry, view in the horizontal plane.

Fig. 3. Result of testing the probing system without plasma formation: *1* – non-delayed probe pulse, *2* – delayed reference pulse without plasma.

Fig. 4. Ratio of the reference pulse I_{ref} to the probe pulse I_{prob} in the absence of probed plasma in the discharger: *1* – non-delayed probe pulse, *2* – reference pulse shifted by 109.6 ns (left axis), *3* – ratio of reference pulse to probe pulse without plasma in the discharger (right axis).

Fig. 5. Distortion of the probe signal introduced by plasma formed by a pulse with minimum energy E_i=55 mJ: *1* – probe pulse passing through plasma, *2* – reference pulse (left axis), *3* – ratio of reference pulse to probe pulse (right axis).

Fig. 6. Superposition of 20 signals obtained during a series of measurements at fixed energy of the triggering laser pulse E_i=55 mJ, $K(t) = I_{ref} / I_{prob}$.

Fig. 7. Calculation of $K_m(t)$ and ΔK at laser pulse energy E_i=55 mJ: *1* – average absorption coefficient K_m (left axis), *2* – ΔK (right axis).

Fig. 8. Calculation $K_m(t)$ and ΔK at laser pulse energy E_i=95.5 mJ: *1* – average absorption coefficient K_m (left axis), *2* – ΔK (right axis).

Fig. 9. Dependence of absorption coefficient K_m on time and laser pulse energy.

Fig. 10. Dependence of absorption coefficient jitter ΔK on time and laser pulse energy.

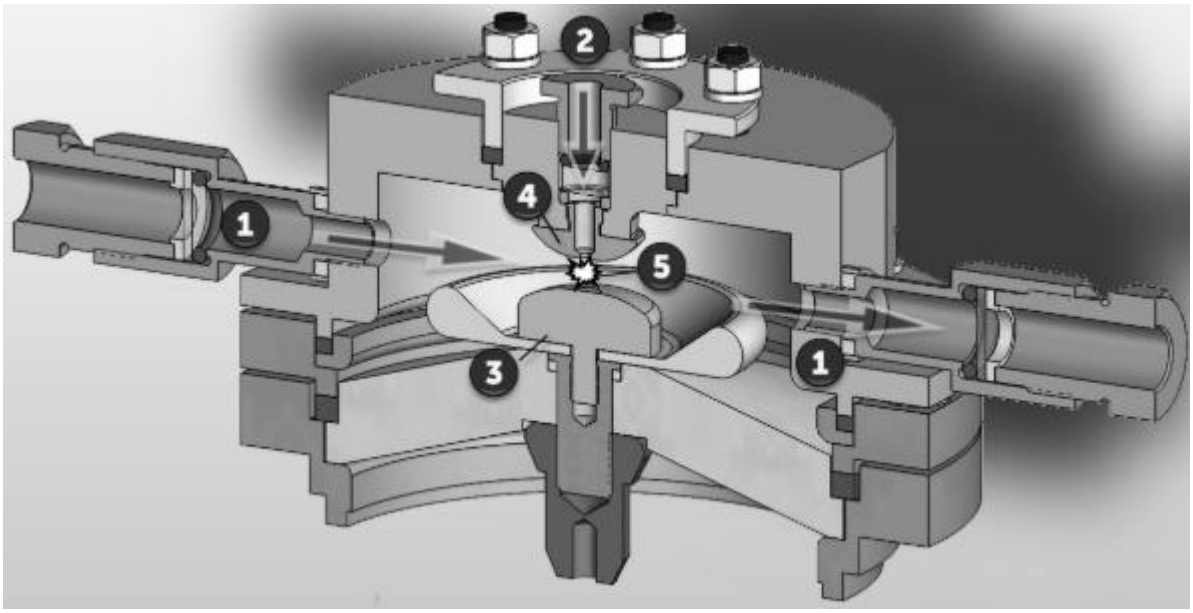

Fig. 1

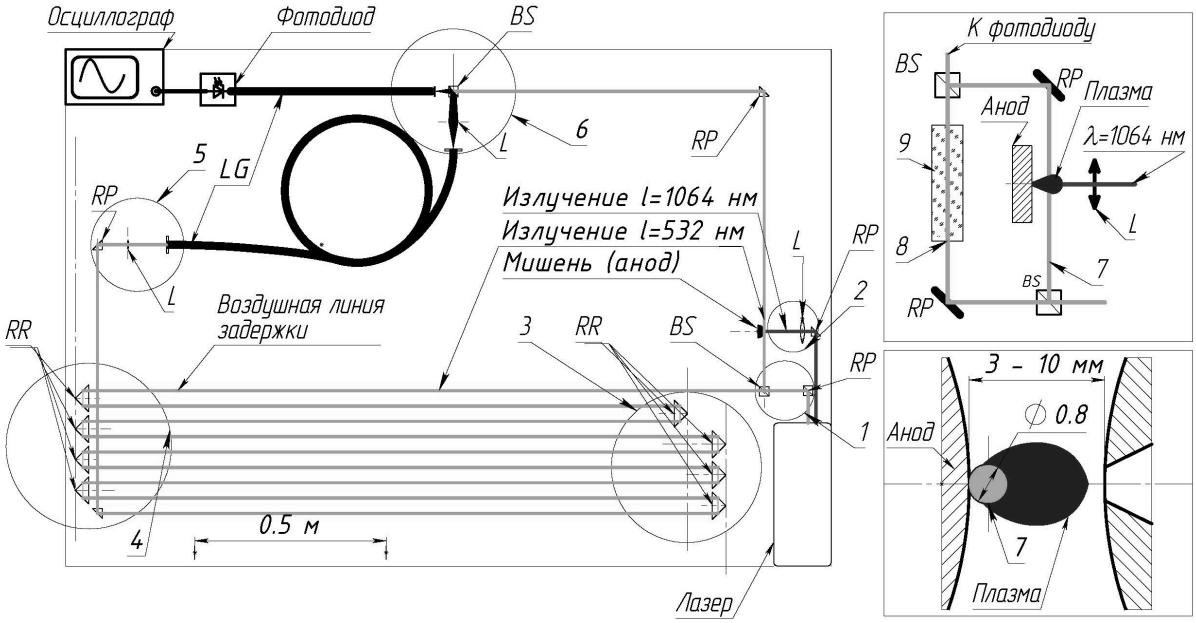
Осциллограф
Фотодиод
BS
6
RP
5
LG
RP
L
Излучение l=1064 нм
Излучение l=532 нм
Мишень (анод)
L
RP
2
Воздушная линия задержки
RR
3
RR
BS
RP
1
RR
4
0.5 м
Лазер
К фотодиоду
BS
RP
Плазма
Анод
λ=1064 нм
9
L
8
7
BS
RP
3 - 10 мм
∅ 0.8
Анод
7
Плазма

Fig.2

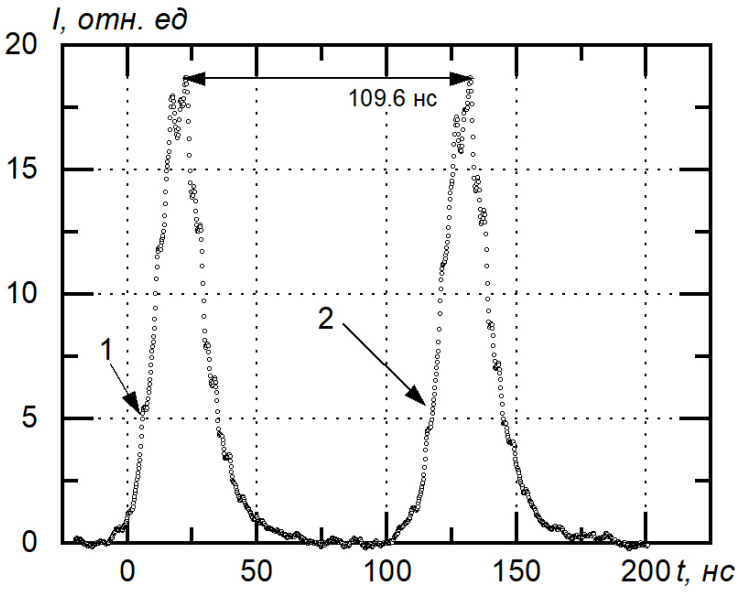
I, отн. ед
20
15
10
5
0
109.6 нс
1
2
0
50
100
150
200
t, нс

Fig.3

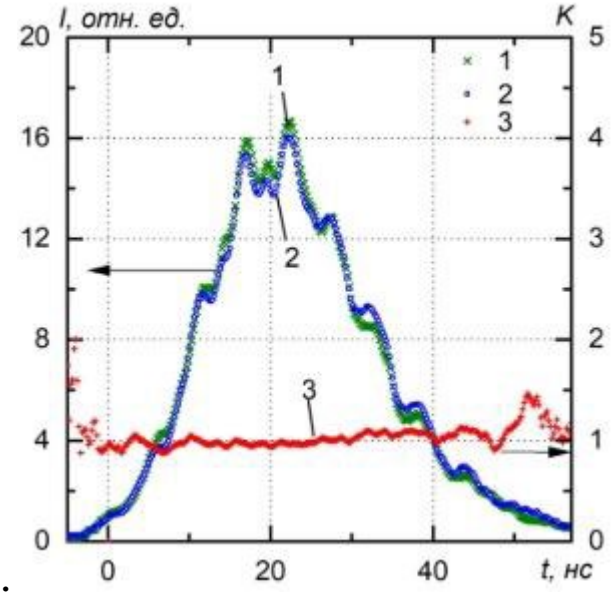

Fig. 4.

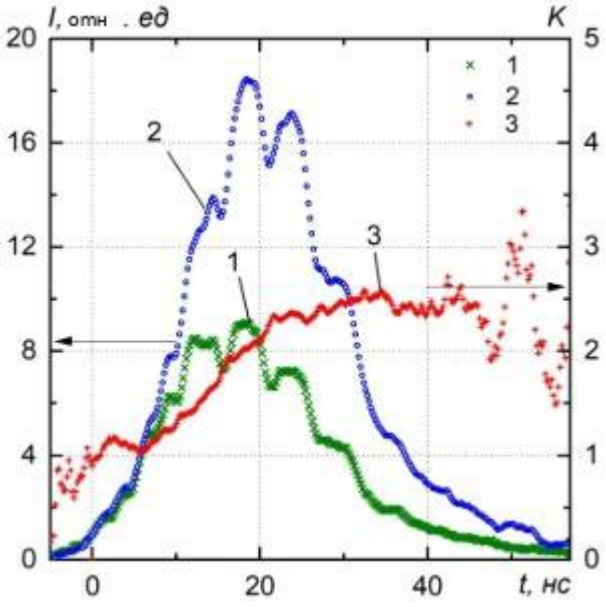

Fig. 5.

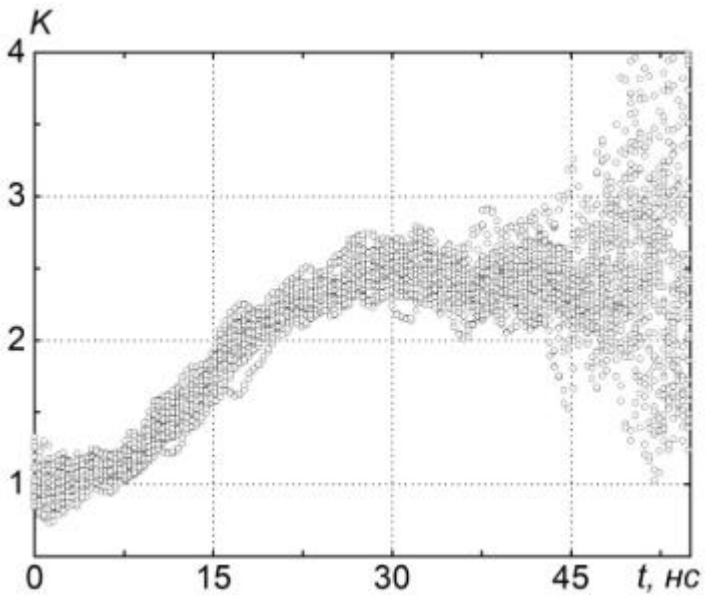

Fig. 6

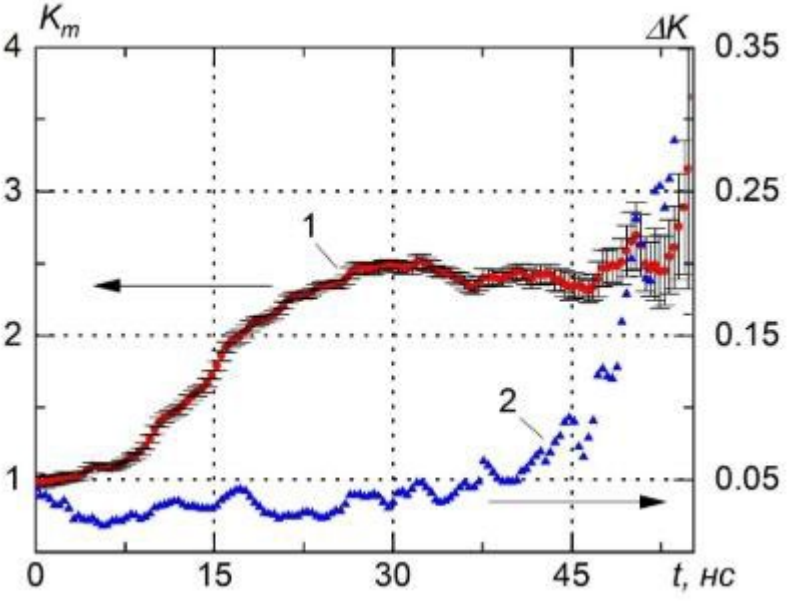

Fig.7

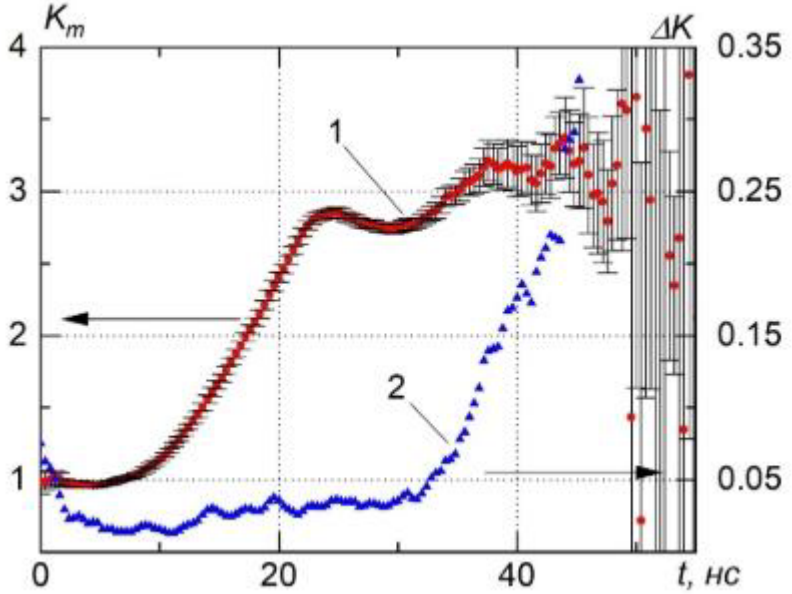
K_m
ΔK
4
3
2
1
0.35
0.25
0.15
0.05
0
20
40
t, нс
1
2

Fig. 8

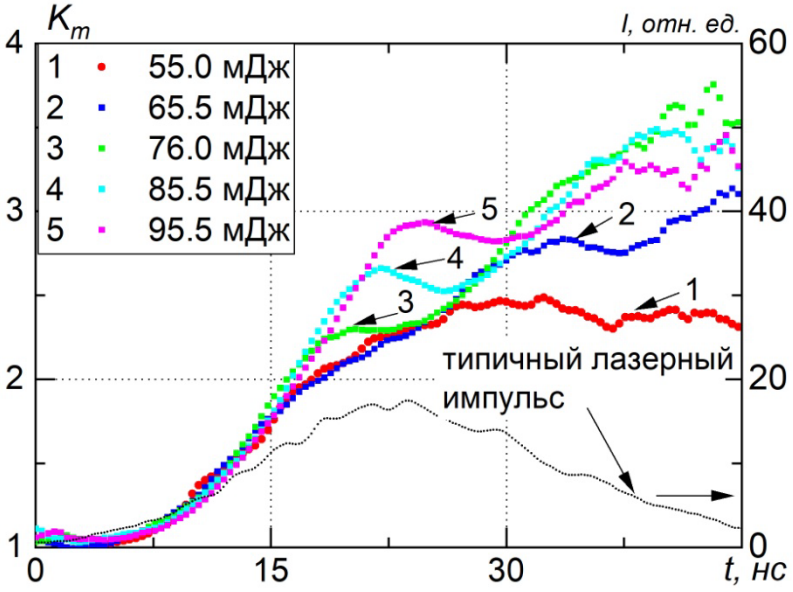
K_m
I, отн. ед.
1 55.0 мДж
2 65.5 мДж
3 76.0 мДж
4 85.5 мДж
5 95.5 мДж
4
3
2
1
60
40
20
0
0
15
30
t, нс
5
2
4
3
1
типичный лазерный импульс

Fig. 9

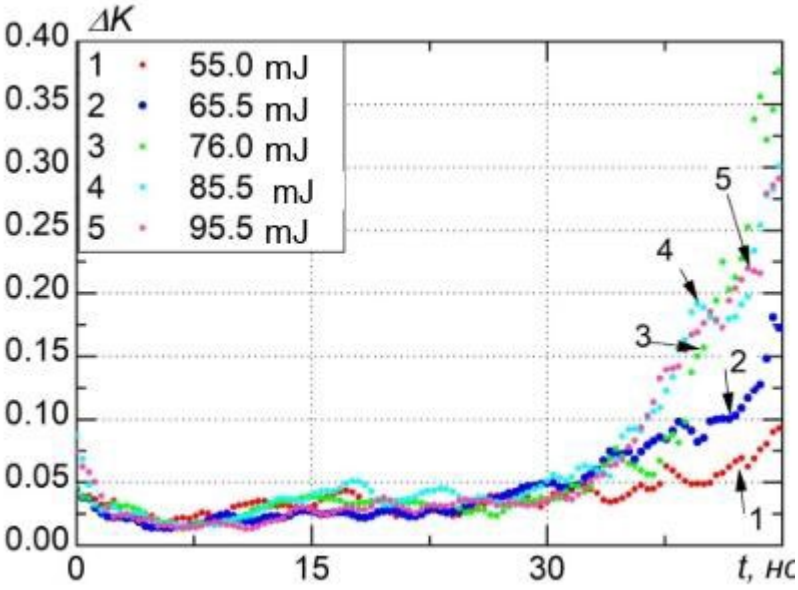
ΔK
0.40
0.35
0.30
0.25
0.20
0.15
0.10
0.05
0.00
1 55.0 mJ
2 65.5 mJ
3 76.0 mJ
4 85.5 mJ
5 95.5 mJ
0
15
30
t, нс
1
2
3
4
5

Fig. 10.